

## Long-Range Coulomb Interactions in Surface Systems: A First-Principles Description within Self-Consistently Combined *GW* and Dynamical Mean-Field Theory

P. Hansmann,<sup>1</sup> T. Ayrál,<sup>1,2</sup> L. Vaugier,<sup>1</sup> P. Werner,<sup>3</sup> and S. Biermann<sup>1,4</sup>

<sup>1</sup>*Centre de Physique Théorique, Ecole Polytechnique, CNRS UMR7644, 91128 Palaiseau, France*

<sup>2</sup>*Institut de Physique Théorique (IPhT), CEA, CNRS, URA 2306, 91191 Gif-sur-Yvette, France*

<sup>3</sup>*Department of Physics, University of Fribourg, 1700 Fribourg, Switzerland*

<sup>4</sup>*Japan Science and Technology Agency, CREST, Kawaguchi 332-0012, Japan*

(Received 17 January 2013; published 16 April 2013)

Systems of adatoms on semiconductor surfaces display competing ground states and exotic spectral properties typical of two-dimensional correlated electron materials which are dominated by a complex interplay of spin and charge degrees of freedom. We report a fully *ab initio* derivation of low-energy Hamiltonians for the adatom systems Si(111):*X*, with *X* = Sn, Si, C, Pb, that we solve within self-consistently combined *GW* and dynamical mean-field theory. Calculated photoemission spectra are in agreement with available experimental data. We rationalize experimentally observed trends from Mott physics toward charge ordering along the series as resulting from substantial long-range interactions.

DOI: [10.1103/PhysRevLett.110.166401](https://doi.org/10.1103/PhysRevLett.110.166401)

PACS numbers: 71.15.-m, 71.10.Fd, 71.30.+h, 73.20.At

Understanding the electronic properties of materials with strong electronic Coulomb correlations remains one of the biggest challenges of modern condensed matter physics. The interplay of delocalization and interactions is not only at the origin of exotic ground states, but also determines the excitation spectra of correlated materials. The “standard model” of correlated fermions, the Hubbard model, in principle captures these phenomena. Yet relating the model to the material on a microscopic footing remains a challenge. Even more importantly, the approximation of purely local Coulomb interactions can become severe in realistic materials, where long-range interactions and charge fluctuation physics cannot be neglected.

Systems of adatoms on semiconducting surfaces, such as Si(111):*X* with *X* = Sn, C, Si, Pb, have been suggested [1] to be good candidates for observing low-dimensional correlated physics. Commonly considered to be realizations of the one-band Hubbard model and toy systems for investigating many-body physics on the triangular lattice, such surfaces have been explored both experimentally [2–18] and theoretically [19–31]. These so-called  $\alpha$  phases show a remarkable variety of interesting physics including commensurate charge density wave states [5,6,9] and isostructural metal to insulator transitions [14]. However, while specific systems and/or phenomena have been investigated also theoretically, a comprehensive understanding including materials trends is still lacking. A central goal of our work is to present a unified picture that relates, within a single framework, different materials (adatom systems), placing them in a common phase diagram.

We derive low-energy effective Hamiltonians *ab initio* from a combined density functional and constrained random phase approximation (cRPA) scheme [32] in the implementation of Ref. [33] (see also the extension to surface systems in Ref. [34]). While the first surprise is

the relatively large value of the on-site interactions, which we find to be of the order of the bandwidth ( $\approx 1$  eV), most importantly we show that nonlocal interactions are large (nearest-neighbor interaction of  $\approx 0.5$  eV) and, hence, an essential part of the resulting many-body Hamiltonians. This result confirms previous speculations about the importance of nonlocal effects in these materials [21,29]. We solve these low-energy Hamiltonians within fully self-consistent combined *GW* and dynamical mean-field theory (*GW* + DMFT) [35], calculating in particular (single-particle) angular resolved photoemission spectra and the (two-particle) charge susceptibility. We identify a clear-cut materials trend starting from Si(111):C deep in a Mott phase to Si(111):Pb which shows tendencies toward metallicity and charge-ordered states driven by nonlocal interactions. Comparing our results to available experimental data yields encouraging insights: *Without adjustable parameters* we reproduce the experimentally measured gap size of insulating Si(111):Sn and its transition to a “bad insulator” at elevated temperatures. Moreover, based on the charge susceptibility, we identify the *electronic* tendency of Si(111):Pb toward charge ordering of the so-called  $3 \times 3$  symmetry, which is indeed seen experimentally by scanning tunneling microscopy. Our work is the first one that addresses the electronic properties of real materials on the basis of fully self-consistent *GW* + DMFT calculations [36] (for a non-self-consistent calculation, see Ref. [37]; for self-consistent calculations for models, see Refs. [38–40]) [41].

The single-particle part of the Hamiltonian is calculated in the local density approximation of density functional theory. In Fig. 1, we present local density approximation band structures for the series Si(111):{C, Si, Sn, Pb}. For all considered systems, the surface state in the semiconducting gap is indeed responsible for a *well-separated*,

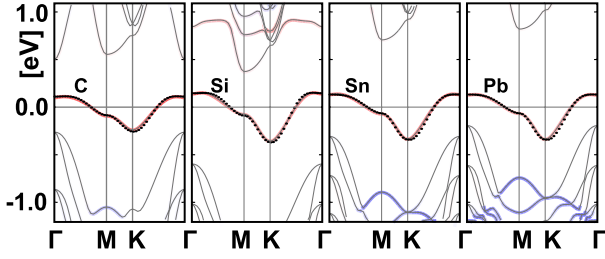


FIG. 1 (color online). Band structures of the  $\alpha\text{-}\sqrt{3} \times \sqrt{3}$  phases of Si(111):X with  $X = \text{Sn, Si, C, Pb}$  [53]. In red (gray) we plot the contributions stemming from the  $p_z$  orbital of the adatom, while the blue (dark gray) color denotes  $p_{x,y}$ -like (i.e., planar) character. Even though the actual molecular orbital composition might be complicated, the half-filled surface band has a clear-cut “apical” (i.e., carrotlike) character. The black dots represent the tight binding relation Eq. (1) with hopping parameters from Table I. The quality of the fit supports the picture of Wannier-like orbitals with a fast decaying real space overlap on neighboring sites.

single band around the Fermi energy. The tight-binding dispersion of the half-filled surface band can be well fitted by using up to third-nearest-neighbor hopping (with  $t$ ,  $t'$ , and  $t''$  from Table I):

$$\begin{aligned} \varepsilon_{\mathbf{k}} = & 2t[\cos(k_x) + 2 \cos(k_x/2) \cos(\sqrt{3}/2k_y)] \\ & + 2t'[\cos(\sqrt{3}k_y) + 2 \cos(3k_x/2) \cos(\sqrt{3}/2k_y)] \\ & + 2t''[\cos(2k_x) + 2 \cos(k_x) \cos(\sqrt{3}k_y)]. \end{aligned} \quad (1)$$

In order to determine the interaction parameters as partially screened matrix elements of the Coulomb interaction within the cRPA, we chose an energy window around the Fermi energy encompassing the surface band. The bare interaction parameters are calculated by means of explicit evaluation of the radial (Slater) integrals of the Wannier functions. The local and nonlocal Hubbard interaction parameters are obtained as the corresponding matrix elements of the partially screened interaction within the cRPA [34]. The cRPA scheme provides us with the full frequency dependence of the interactions. Up to the energy scale of the plasma frequency of silicon, however, this frequency dependence is small and will be neglected in the following. The resulting static effective interactions are summarized in Table I.

The bare on-site interaction parameters ( $V_0$ ) vary between 6.0 eV for Si(111):C and 4.3 eV for Si(111):Pb, decreasing monotonically within the series. The on-site  $U_0$  is reduced roughly by a factor of 4–5 due to cRPA screening. At first glance the on-site  $U_0$  of the order of 1 eV—about twice the size of the bandwidth—strongly points toward Mott physics. This is, however, a premature conclusion due to the effect of *nonlocal* interactions. The first nonlocal contribution (nearest-neighbor interaction)  $U_1$  (bare  $V_1$ ) is 0.5 eV (2.8 eV). Remarkably, the value is—in contrast to  $U_0$  ( $V_0$ )—almost the same for all materials.

TABLE I. Values of the bare (effective) on-site  $V_0$  ( $U_0$ ) and intersite  $V_1$  ( $U_1$ ) interactions. Also reported are the values of the static component of the effective  $\mathcal{U}(\omega = 0)$  calculated from GW + DMFT; see the text.

	C	Si	Sn	Pb
$t$ (meV)	38.0	50.0	42.0	42.0
$-t'$ (meV)	15.0	23.0	20.0	20.0
$t''$ (meV)	0.5	5.0	10.0	10.0
$U_0$ (eV)	1.4	1.1	1.0	0.9
$U_1$ (eV)	0.5	0.5	0.5	0.5
$U_n$	$U_1/r_a$	$U_1/r_a$	$U_1/r_a$	$U_1/r_a$
$V_0$ (eV)	6.0	4.7	4.4	4.3
$V_1$ (eV)	2.8	2.8	2.7	2.8
$V_1/\varepsilon_{\text{Si surf.}}^{\text{stat.}}$ (eV)	0.47	0.47	0.45	0.47
$\mathcal{U}(\omega = 0)$ (eV)	1.3	0.94	0.84	0.67 (ins.) 0.54 (met.)

The reason is that the intersite overlap of the orbitals is so small that the Coulomb energy corresponds to the electrostatic energy of two point charges. With the virial theorem  $\langle E^{\text{tot.}} \rangle = 1/2\langle V \rangle$ , we quantify this argument by a rescaled hydrogen problem with effective Bohr radius of 12 a.u. ( $\approx$  distance of adatom sites),

$$\left\langle \frac{e^2}{r_{\text{rel}}} \right\rangle = \frac{1}{12} |V_{\text{pot}}^{\text{H-atom}}| = \frac{1}{12} 2 |E_{\text{groundstate}}^{\text{H-atom}}| = 2.3 \text{ eV}, \quad (2)$$

which roughly matches the value of our bare intersite interaction parameters. The second, likewise remarkable, observation is that the screened values  $U_1$  are extremely close to the value we get by assuming a static continuum approximation on the surface of a dielectric medium:  $V_1/\varepsilon_{\text{Si}}^{\text{surf}}$ , where  $\varepsilon_{\text{Si}}^{\text{surf}} = \frac{1}{2}(\varepsilon_{\text{Si}} + 1)$  is the static dielectric constant of silicon on the surface. The reason is straightforward: The adatom distance (6 Å) is already large enough compared to the atomic structure of the silicon substrate ( $\approx 2$  Å) so that *local field effects* (included in the cRPA) are negligible. Following this reasoning, we can calculate longer-range interaction terms by simply scaling  $U_1$  with  $a/r$ , i.e., with the inverse distance in units of the nearest-neighbor distance  $a$ , i.e.,  $U_2 = U_1/\sqrt{3}$  and so on. In this respect,  $U_1$  is not only the nearest-neighbor interaction, but the parameter that quantifies the strength of nonlocal interactions. The many-body Hamiltonian resulting from our *parameter-free* downfolding procedure thus reads

$$H = \sum_{\mathbf{k}, \sigma} \varepsilon_{\mathbf{k}} c_{\mathbf{k}, \sigma}^\dagger c_{\mathbf{k}, \sigma} + \sum_i U_0 n_{i, \uparrow} n_{i, \downarrow} + \sum_{i \neq j} U_{|i-j|} n_i n_j, \quad (3)$$

where  $\varepsilon_{\mathbf{k}}$  is the dispersion relation (1),  $c_{\mathbf{k}, \sigma}^\dagger$  ( $c_{\mathbf{k}, \sigma}$ ) are fermionic creation (annihilation) operators,  $n_{i, \sigma}$  is the number operator counting electrons in the  $p_z$ -like Wannier orbital centered at adatom  $i$ , and  $n_i = n_{i, \uparrow} + n_{i, \downarrow}$ .

To solve this Hamiltonian, we implement the combined GW + DMFT scheme [35,44] and calculate spectral

properties and charge-charge response functions. Fully self-consistent  $GW + DMFT$  was applied to the extended Hubbard model in the seminal work by Sun and Kotliar [38,45], but only recently have numerical techniques for the solution of dynamical impurity models [47–49] been sufficiently advanced to extract real-frequency information from such calculations [39,40]. We employ the techniques of the latter two works (in particular, a continuous-time quantum Monte Carlo impurity solver based on the hybridization expansion [47]) but implement them for the realistic Hamiltonian derived above. Moreover, we go beyond the “standard” extended Hubbard model and do not restrict the range of the nonlocal interaction terms. Rather, we include the entire  $1/r$  tail by means of an Ewald-type lattice sum. In Fig. 2, we show momentum-resolved spectral functions from  $GW + DMFT$  for all compounds in our series: As expected from the large on-site interactions compared to the bandwidth, we obtain insulating spectra for all four compounds. Interestingly, however, for the Pb compound, in contrast to the other three systems, we find, depending on the initialization, two stable solutions at the temperature of our study ( $T = 116$  K)—one metallic and one insulating. This indicates that we are in a coexistence region of a first-order phase transition similar to that seen in the extended Hubbard model [40].

In all compounds, the upper and lower Hubbard bands show a substantial dispersion following the bare band structure, as would be expected from an atomic limit estimate. The insulating gap decreases within the series, and we can estimate from the center of mass of the

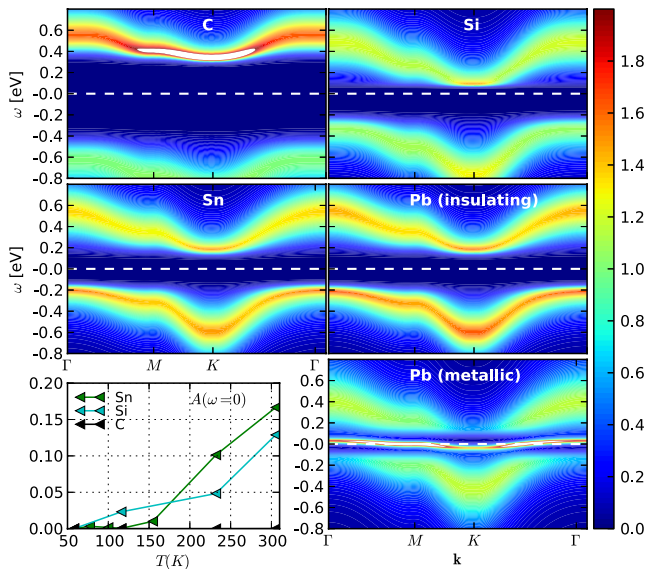


FIG. 2 (color online). Momentum-resolved spectral function at  $T = 116$  K of  $\text{Si}(111):X$  with  $X = \text{Sn}, \text{Si}, \text{C}, \text{Pb}$  obtained by analytical continuation of  $GW + DMFT$  imaginary-time data. The Fermi energy is set to  $\varepsilon_F = 0$  and indicated by the white dashed line. On the bottom left, we show the spectral weight at the Fermi energy as a function of temperature.

Hubbard band values of 1.3 (C), 0.8 (Si), 0.7 (Sn), and 0.5 eV (Pb). However, specifically for the  $\text{Si}(111):\{\text{Sn}, \text{Pb}\}$  we find substantial spectral weight already at  $\geq -0.2$  eV. Given this small gap, a sizable temperature dependence can be expected. We have extracted the value of the local (i.e.,  $\mathbf{k}$ -integrated) spectral function at the Fermi level [50] (see Fig. 2, bottom left panel). While for  $\text{Si}(111):\text{C}$  the spectral weight transfer to the Fermi energy with temperature is negligible as expected from the larger gap, specifically  $\text{Si}(111):\text{Si}$  and most of all  $\text{Si}(111):\text{Sn}$  display a significant transfer of spectral weight on a temperature scale from 50 K to room temperature 300 K.

Photoemission experiments for  $\text{Si}(111):\text{Sn}$  [10,18] (and, possibly Ref. [51], for  $\text{Si}(111):\text{Pb}$  [11]) observe, indeed, such a temperature dependence and agree well with our findings, both concerning the gap size and temperature scale. Our results—obtained *without any adjustable parameters*—also provide theoretical predictions for more extensive studies on  $\text{Si}(111):\text{Pb}$  and the (experimentally so far not studied)  $\text{Si}(111):\text{C}$  compound. Next, we analyze the spectral functions in view of the interaction strengths calculated by cRPA (see Table I). The gap sizes no longer reflect the energy scale of the on-site interaction  $U_0$  but are reduced due to nonlocal interactions which *screen* the local interaction by nonlocal charge fluctuations. This physics is naturally present in the  $GW + DMFT$  scheme, where nonlocal effects are incorporated into an effective retarded on-site interaction  $\mathcal{U}(\omega)$  (plotted in the left panel of Fig. 3). The dynamical character of this quantity results from downfolding of nonlocal degrees of freedom and is not to be confused with the frequency dependence of effective interactions within cRPA [32] (neglected here—see above). The latter results from downfolding higher energy (orbital) degrees of freedom. The shape of the  $GW + DMFT$   $\mathcal{U}(\omega)$  is reminiscent of the latter, but the energy scales are drastically reduced.

At large frequencies, screening is not efficient and, hence,  $\mathcal{U}(\omega = \infty) = U_0$ . On the other hand, the static value  $\mathcal{U}(\omega = 0)$  can be significantly reduced [up to nearly a factor of 2 for  $\text{Si}(111):\text{Pb}$ ]. The latter sets the energy scale for the gaps we observe in the spectral function. The

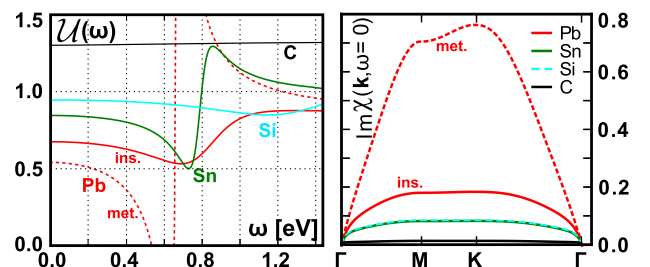


FIG. 3 (color online). Left: frequency-dependent  $\mathcal{U}(\omega)$  (calculated from  $GW + DMFT$ ) including both insulating and metallic cases for the Pb system. Right: imaginary part of the charge-charge susceptibility along the usual path in the Brillouin zone.

transition between unscreened high-frequency behavior and the static value takes place at an energy scale  $\omega_0$  characteristic of charge fluctuations driven by nonlocal interactions. The strikingly different behavior of the dynamical effective interactions  $\mathcal{U}(\omega)$  reflects the observed materials trend: Si(111):C [Si(111):Si] is [nearly] unaffected by nonlocal interaction terms, and there is barely any screening. The remaining two compounds show, however, large effects. The static values  $\mathcal{U}(\omega = 0)$  are reduced compared to the on-site interaction to 0.84 eV for Si(111):Sn and to 0.67 eV (0.54 eV) for the insulating (metallic) solution for Si(111):Pb, which leads to the reduced gap sizes. Moreover, resonances at energies between 0.6 and 0.8 eV stress the importance of nonlocal interactions and charge fluctuations for these systems.

Besides leading to a retarded, frequency-dependent interaction, the nonlocal charge fluctuations signal tendencies toward a charge-ordered state. Analyzing the momentum dependence of the imaginary part of the charge-charge response function  $\text{Im}\chi(\mathbf{k}, \omega = 0)$  for the high-symmetry points of the Brillouin zone, shown in Fig. 3, we find for the different materials a very characteristic behavior. The local double occupancy, which corresponds to the integral of the plotted quantity over all momenta, becomes larger toward the end of the series. Most interesting is the case of metallic Si(111):Pb for which we find a distinct structure within the Brillouin zone: The maximum of  $\text{Im}\chi(\mathbf{k}, \omega = 0)$  at the  $K$  symmetry point indicates strong charge fluctuations of the so-called  $3 \times 3$  symmetry, sketched in Fig. 4. This order might eventually be frozen in to form a charge-ordered ground state which is actually seen in scanning tunneling microscopy for this material [8]. An insulating charge-ordered ground state of  $3 \times 3$  symmetry is, in fact, also found in Ge(111):Sn [52], where a concomitant structural distortion (vertical displacement of adatoms) of the same symmetry is seen. Our results show that the instability in the correlated electronic response function may play a key role in this physics.

We can summarize our results by drawing a schematic phase diagram as a function of the strength of local and nonlocal interactions (represented by the value of  $U_1$ ); see Fig. 4. For zero nonlocal interactions, our phase diagram describes the Mott-Hubbard metal to insulator transition. The adatom systems are placed at about 0.5 eV of nonlocal interaction strength. However, due to the difference in the on-site term  $U_0$  their respective position in the phase diagram and, hence, their ground state character are different: Si(111):C is deep in the Mott phase with a charge localization with one electron per adatom site. The Si(111):Si compound [53] is also of Mott type with only small values for the double occupancy and little effect of charge fluctuations. However, Si(111):Sn and, most dramatic, Si(111):Pb (which is actually already in a coexistence region) are much closer to a phase boundary to a metallic phase. Even more peculiar is the obvious tendency

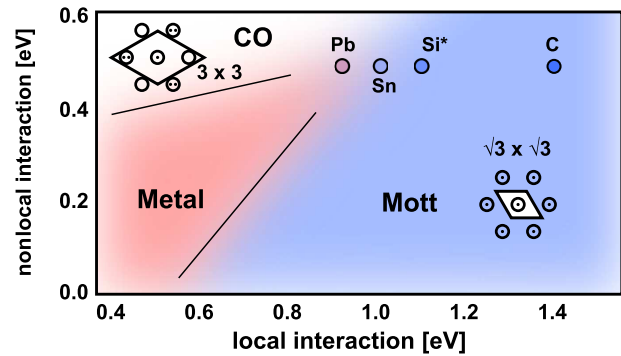


FIG. 4 (color online). Schematic local-nonlocal interaction phase diagram: The black-bordered circles mark the positions of the adatom systems of our study. Straight lines are guides to the eyes, and blurry color indicates coexistence regions. Within the localized (i.e., insulating) phases CO and Mott, small sketches indicate the shape of the surface unit cell.

of Si(111):Pb toward a charge-ordered phase of  $3 \times 3$  symmetry indicated by the white region in our phase diagram.

In conclusion, we have set up a fully self-consistent  $GW + \text{DMFT}$  scheme for the realistic treatment of correlated surface systems to address the electronic properties of the  $\alpha$  phases of adatoms on the Si(111) surface. We have reported on the *ab initio* construction of the materials-specific low-energy Hamiltonians and, most importantly, on the respective interaction parameters including the long-range Coulomb tail. From these, it becomes clear that for the adatom systems, taking into account nonlocal interaction effects is mandatory. We have solved the derived many-body Hamiltonians and discussed our findings for momentum-resolved spectral functions, to be compared to angular resolved photoemission spectra. Without adjustable parameters we have reproduced experimental findings or, in cases where experiments are missing, made predictions. Specifically, the angular resolved photoemission spectra for the series, as well as the charge order instabilities in the case of Si(111):Pb, are key conclusions which can provide guidance for further experimental and theoretical studies of semiconductor adatom structures.

We acknowledge useful discussions with the authors of Refs. [17,18], as well as with M. Capone, M. Casula, H. Hafermann, H. Jiang, M. Katsnelson, O. Parcollet, and E. Tosatti. This work was supported by the French ANR under project SURMOTT and IDRIS/GENCI under Project No. 129313.

- 
- [1] E. Tosatti and P. W. Anderson, Jpn. J. Appl. Phys. **2S2**, 381 (1974).
  - [2] R.I.G. Uhrberg, G. V. Hansson, J.M. Nicholls, P.E. S. Persson, and S.A. Flodström, Phys. Rev. B **31**, 3805 (1985).

- [3] T.M. Grehk, L.S.O. Johansson, U.O. Karlsson, and A.S. Flödstrom, *Phys. Rev. B* **47**, 13887 (1993).
- [4] H.H. Weitering, J. Chen, N.J. DiNardo, and E.W. Plummer, *Phys. Rev. B* **48**, 8119 (1993).
- [5] J.M. Carpinelli, H.H. Weitering, E.W. Plummer, and R. Stumpf, *Nature (London)* **381**, 398 (1996).
- [6] J.M. Carpinelli, H.H. Weitering, M. Bartkowiak, R. Stumpf, and E.W. Plummer, *Phys. Rev. Lett.* **79**, 2859 (1997).
- [7] H.H. Weitering, X. Shi, P.D. Johnson, J. Chen, N.J. DiNardo, and K. Kempa, *Phys. Rev. Lett.* **78**, 1331 (1997).
- [8] J. Slezák, P. Mutombo, and V. Cháb, *Phys. Rev. B* **60**, 13328 (1999).
- [9] G.L. Lay, M.G. Rad, M. Gthelid, U. Karlsson, J. Avila, and M. Asensio, *Appl. Surf. Sci.* **175–176**, 201 (2001).
- [10] J. Lobo, A. Tejada, A. Mugarza, and E.G. Michel, *Phys. Rev. B* **68**, 235332 (2003).
- [11] V. Dudr, N. Tsud, S. Fabík, B. Ressel, M. Vondráček, K.C. Prince, V. Matolín, and V. Cháb, *Surf. Sci.* **566–568**, 804 (2004).
- [12] C.A. Pignedoli, A. Catellani, P. Castrucci, A. Sgarlata, M. Scarselli, M. De Crescenzi, and C.M. Bertoni, *Phys. Rev. B* **69**, 113313 (2004).
- [13] M.H. Upton, T. Miller, and T.-C. Chiang, *Phys. Rev. B* **71**, 033403 (2005).
- [14] S. Modesti, L. Petaccia, G. Ceballos, I. Vobornik, G. Panaccione, G. Rossi, L. Ottaviano, R. Larciprete, S. Lizzit, and A. Goldoni, *Phys. Rev. Lett.* **98**, 126401 (2007).
- [15] L.A. Cardenas, Y. Fagot-Revurat, L. Moreau, B. Kierren, and D. Malterre, *Phys. Rev. Lett.* **103**, 046804 (2009).
- [16] T. Zhang, P. Cheng, W.-J. Li, Y.-J. Sun, G. Wang, X.-G. Zhu, K. He, L. Wang, X. Ma, X. Chen, Y. Wang, Y. Liu, H.-Q. Lin, J.-F. Jia, and Q.-K. Xue, *Nat. Phys.* **6**, 104 (2010).
- [17] C. Tournier-Colletta, L. Cardenas, Y. Fagot-Revurat, A. Tejada, B. Kierren, and D. Malterre, *Phys. Rev. B* **84**, 155443 (2011).
- [18] G. Li, P. Höpfner, J. Schäfer, C. Blumenstein, S. Meyer, A. Bostwick, E. Rotenberg, R. Claessen, and W. Hanke, *Nat. Commun.* **4**, 1620 (2013).
- [19] E. Kaxiras, K.C. Pandey, F.J. Himpsel, and R.M. Tromp, *Phys. Rev. B* **41**, 1262 (1990).
- [20] K.D. Brommer, M. Needels, B.E. Larson, and J.D. Joannopoulos, *Phys. Rev. Lett.* **68**, 1355 (1992).
- [21] G. Santoro, S. Scandolo, and E. Tosatti, *Phys. Rev. B* **59**, 1891 (1999).
- [22] C.S. Hellberg and S.C. Erwin, *Phys. Rev. Lett.* **83**, 1003 (1999).
- [23] H. Aizawa, M. Tsukada, N. Sato, and S. Hasegawa, *Surf. Sci.* **429**, L509 (1999).
- [24] G. Profeta, A. Continenza, L. Ottaviano, W. Mannstadt, and A.J. Freeman, *Phys. Rev. B* **62**, 1556 (2000).
- [25] H.Q. Shi, M.W. Radny, and P.V. Smith, *Phys. Rev. B* **66**, 085329 (2002).
- [26] H.Q. Shi, M.W. Radny, and P.V. Smith, *Phys. Rev. B* **70**, 235325 (2004).
- [27] G. Profeta and E. Tosatti, *Phys. Rev. Lett.* **95**, 206801 (2005).
- [28] G. Profeta and E. Tosatti, *Phys. Rev. Lett.* **98**, 086401 (2007).
- [29] S. Schuwalow, D. Grieger, and F. Lechermann, *Phys. Rev. B* **82**, 035116 (2010).
- [30] L. Chaput, C. Tournier-Colletta, L. Cardenas, A. Tejada, B. Kierren, D. Malterre, Y. Fagot-Revurat, P. Le Fèvre, F. Bertran, A. Taleb-Ibrahimi, D.G. Trabada, J. Ortega, and F. Flores, *Phys. Rev. Lett.* **107**, 187603 (2011).
- [31] G. Li, M. Laubach, A. Fleszar, and W. Hanke, *Phys. Rev. B* **83**, 041104 (2011).
- [32] F. Aryasetiawan, M. Imada, A. Georges, G. Kotliar, S. Biermann, and A.I. Lichtenstein, *Phys. Rev. B* **70**, 195104 (2004).
- [33] L. Vaugier, H. Jiang, and S. Biermann, *Phys. Rev. B* **86**, 165105 (2012).
- [34] P. Hansmann, L. Vaugier, H. Jiang, and S. Biermann, *J. Phys. Condens. Matter* **25**, 094005 (2013).
- [35] S. Biermann, F. Aryasetiawan, and A. Georges, *Phys. Rev. Lett.* **90**, 086402 (2003).
- [36] We stress again, however, that our calculations are performed for the low-energy effective Hamiltonian, not directly in the continuum.
- [37] J. Tomczak, M. Casula, T. Miyake, F. Aryasetiawan, and S. Biermann, *Europhys. Lett.* **100**, 67001 (2012).
- [38] P. Sun and G. Kotliar, *Phys. Rev. Lett.* **92**, 196402 (2004).
- [39] T. Ayrál, P. Werner, and S. Biermann, *Phys. Rev. Lett.* **109**, 226401 (2012).
- [40] T. Ayrál, S. Biermann, and P. Werner, *Phys. Rev. B* **87**, 125149 (2013).
- [41] We also mention attempts of simplified combined schemes using static screened interactions in Refs. [35,42,43].
- [42] K. Karlsson, *J. Phys. Condens. Matter* **17**, 7573 (2005).
- [43] C. Taranto, M. Kaltak, N. Parragh, G. Sangiovanni, G. Kresse, A. Toschi, and K. Held, [arXiv:1211.1324](https://arxiv.org/abs/1211.1324).
- [44] S. Biermann, F. Aryasetiawan, and A. Georges, *Proceedings of the NATO Advanced Research Workshop on Physics of Spin in Solids: Materials, Methods, and Applications, Azerbaijan, 2003*, NATO Science Series II Vol. 156 (Kluwer, Dordrecht, 2004), p. 43.
- [45] See also Ref. [46] for a variant of the GW + DMFT scheme.
- [46] P. Sun and G. Kotliar, *Phys. Rev. B* **66**, 085120 (2002).
- [47] P. Werner and A.J. Millis, *Phys. Rev. Lett.* **104**, 146401 (2010).
- [48] P. Werner, M. Casula, T. Miyake, F. Aryasetiawan, A. Millis, and S. Biermann, *Nat. Phys.* **8**, 331 (2012).
- [49] M. Casula, A. Rubtsov, and S. Biermann, *Phys. Rev. B* **85**, 035115 (2012).
- [50] From the imaginary-time Green's function at  $G(\tau = \beta/2)$ .
- [51] It is experimentally difficult to determine the symmetry of the Si(111):Pb ground state—this challenge can, in fact, be explained by our results of charge order instabilities.
- [52] J. Avila, A. Mascaraque, E.G. Michel, M.C. Asensio, G. LeLay, J. Ortega, R. Perez, and F. Flores, *Phys. Rev. Lett.* **82**, 442 (1999).
- [53] The structure Si(111):Si is a hypothetical structure—it is not stable in the  $\sqrt{3} \times \sqrt{3}$  phase.